Finite-temperature infrared and Raman spectra of high-pressure hydrogen from first-principles molecular dynamics

Chunyi Zhang,[1] Cui Zhang,[2] Mohan Chen,[3] Wei Kang,[1,4,*] Zhuowei Gu,[5] Jianheng Zhao,[5] Cangli Liu,[5] Chengwei Sun,[5] and Ping Zhang[1,2,†]

[1]*HEDPS, Center for Applied Physics and Technology, College of Engineering, Peking University, Beijing 100871, China*
[2]*Institute of Applied Physics and Computational Mathematics, Beijing 100088, China*
[3]*Department of Physics, Temple University, Philadelphia, Pennsylvania 19122, USA*
[4]*Collaborative Innovation Center of IFSA, Shanghai Jiao Tong University, Shanghai 200240, China*
[5]*Institute of Fluid Physics, China Academy of Engineering Physics, Mianyang 621900, China*

(Received 25 June 2018; revised manuscript received 12 September 2018; published 1 October 2018)

Finite-temperature infrared and Raman spectra of theoretically proposed stable structures $C2/c$ and Pc of high-pressure solid hydrogen are calculated from time correlation functions of dipole moments and polarizabilities extracted from first-principles molecular dynamics simulations. Calculated spectra are much improved compared with those obtained from density functional perturbation theory at zero temperature, which suggests the significance of finite-temperature effects in both spectra. The excellent agreement between the calculated spectra of the $C2/c$ structure and experimental results supports the theory that $C2/c$ is the structure of phase III. The high-frequency Raman vibron mode of the Pc structure is also well reproduced compared with experimental spectra. However, the energy of the low-frequency Raman vibron mode of the Pc structure is underestimated up to 16%. This suggests that the atomic structure of the strongly bonded layer in phase IV is well predicted, while the weakly bonded layer still differs from the real structure somehow. In addition, we find that diffusion in the weakly bonded layer of the Pc structure is strong and the layer displays several features of a two-dimensional liquid.

DOI: 10.1103/PhysRevB.98.144301

I. INTRODUCTION

Understanding high-pressure structures of hydrogen has become a focus in condensed-matter physics under extreme conditions [1–3]. However, the structure of high-pressure solid hydrogen [4–8], especially that of metallic hydrogen [9,10], is not fully understood yet. It is difficult to determine structures of high-pressure hydrogen with x-ray diffraction because the scattering intersection of hydrogen is small. Therefore, infrared (IR) and Raman vibrational spectroscopies have become the main tool to study the structure of high-pressure hydrogen.

The phase boundaries of high-pressure solid-hydrogen phases I, II, III, and IV have been identified in experiments by IR and Raman spectra [1,4–8]. Phase I of hydrogen is a low-pressure phase that is stable up to 180 GPa at room temperature [1]. Phase II of hydrogen is a broken-symmetry phase and is stable within 70–160 GPa below 135 K [1]. Phase III of hydrogen was first revealed in experiment from the abrupt discontinuity in the Raman vibron frequency at 145 GPa and 77 K [11]. Subsequent experiments demonstrated that phase III is stable at 285 GPa or higher pressure [12,13]. Phase IV is considered to be a high-temperature entropy-driven phase, which was first revealed by observing two unique strong vibrational Raman modes above 220 GPa at room temperature [5]. Recent experiments suggested several new phases, including phases IV′ [8,14], V [8,14], and VI [13] from changes in Raman spectra, but the existence of these new phases is still under intense debate [13,15].

Among all of the observed phases, only the crystalline structure of the low-pressure phase I is confirmed as a hcp structure with freely rotating molecules at each lattice point [16]. Akahama *et al.* [17] found that in phases II and III, H_2 molecules were in the vicinity of the hcp lattice point, but the exact orientation of H_2 was still unknown. The structural information of other phases is not accessible from experiments so far.

Energetic calculation based on density functional theory (DFT) [18] has been used to rationalize and interpret experimental measurements. It was also used as a prediction tool to provide candidate structures. For instance, the zero-temperature phase diagram [19–22] and a few candidate structures, such as the $P6_3/m$, $Pca2_1$, $P2_1/c$, $C2/c$, $Pbcn$, $Ibam$, Pc, $Cmca$, and $Cmca$-12 structures, have been predicted using the DFT [18] method together with *ab initio* random structure searching (AIRSS) [19,20,23,24].

It would thus be of great help if the IR and Raman spectra of those candidate structures could be calculated and compared with experimental results directly. This would provide a critical approach to identify the structure of hydrogen solids under conditions in which the enthalpies of candidate structures are close.

These spectra were previously calculated [19–21] using the density functional perturbation theory [25] (DFPT) method.

*weikang@pku.edu.cn
†zhang_ping@iapcm.ac.cn

However, at finite temperature, the method neglects, or only partially includes, the temperature effect of protons and thus cannot get the correct linewidth of the spectra. Moreover, some frequencies calculated at zero temperature differ remarkably from experiments when the temperature effect is crucial [26,27], especially for phase IV, which is entropy driven [20] with intrinsic diffusion [28].

Some efforts have been made to include finite-temperature effects [26,27]. For example, Singh *et al.* [27] utilized the DFPT method to get the finite-temperature IR and Raman spectra by averaging 200 configurations selected from a first-principles molecular dynamics (FPMD) simulation. However, the number of configurations, as we shall show in Sec. II, is not enough to converge the spectrum calculation. Magdău and Ackland [26] tried to extract Raman spectra from the projection of velocities taken from FPMD simulations over the stretching mode. However, their method somehow arrived at a vibrational spectrum that differs from the Raman or IR spectrum [29] when electronic, intermolecular, or interlayer effects were not fully included. In addition, Liu *et al.* [28] pointed out that the results of Magdău and Ackland [26] might not be reliable due to very short simulation time (0.25–1.5 ps for the 768-atom Pc cell).

In this work, we calculate the finite-temperature IR and Raman spectra by Fourier transforms of the time correlation functions (TCFs) of the FPMD-extracted dipole moments and polarizabilities, which are computationally expensive but can be compared directly with experimental spectra. In particular, we focus on phases III and IV of high-pressure solid hydrogen, as displayed in Fig. 1, whose existence has been experimentally confirmed [5,11] and which have less remarkable quantum effects than phases I and II[30–33]. Our results support the theory that the $C2/c$ structure is the crystal structure of phase III, while the Pc structure differs from the real structure of phase IV in atomic configurations. At least the comparison of the Raman spectra shows that the H_2 molecules in the weakly bonded layer of phase IV should be about 16%–6% stronger than that in the Pc structure from 210 to 270 GPa.

The rest of this paper is organized as follows. We present the methods in Sec. II and discuss the results in Sec. III. Finally, we conclude our work with a short summary in Sec. IV.

II. METHODOLOGY AND NUMERICAL DETAILS

A. Infrared and Raman spectra

Derived from the Fermi's golden rule, the intensities of IR and Raman spectra are proportional to the Fourier transforms of the TCFs of dipole moments and polarizabilities of the system, respectively, which can be expressed as [34]

$$I^{IR}(\omega) \propto \int \langle \boldsymbol{M}(0) \cdot \boldsymbol{M}(t) \rangle e^{-i\omega t} dt \tag{1}$$

and

$$I^{Raman}(\omega) \propto \int \langle \boldsymbol{\alpha}(0) \cdot \boldsymbol{\alpha}(t) \rangle e^{-i\omega t} dt, \tag{2}$$

where $\boldsymbol{M}(t)$ and $\boldsymbol{\alpha}(t)$ are the dipole moment and polarizability of the system at time t, respectively, ω is the frequency, and $\langle \cdots \rangle$ represents the ensemble average. In the calculation of the Raman spectra for a single layer in the Pc structure, which is used in our analyses, $\boldsymbol{\alpha}(t)$ represents the polarization of the single layer.

The dipole moment in Eq. (1) is extracted every ten steps from FPMD trajectories by computing the maximally localized Wannier functions [35,36]. The polarizability in Eq. (2) is calculated by applying a small electric field $\delta D_j (j = \pm x, \pm y, \pm z)$ to the system in the j direction every ten steps. These six different electric fields induce six different dipole moments $\delta M_i(\delta D_j)$. The polarizability tensor can be calculated using the finite difference $\alpha_{ij} = \frac{\delta M_i(\delta D_{+j}) - \delta M_i(\delta D_{-j})}{2\delta D_j}$. To ensure the convergence of both spectra, the $I^{IR}(\omega)$ and $I^{Raman}(\omega)$ presented are averaged with about 5000 independent calculations. For more details of on-the-fly calculations of dipole moments and polarizabilities in FPMD, the reader is referred to Ref. [37]. The electric field δD_j is chosen to be 0.001 a.u. (1 a.u. $= 5.1422 \times 10^{11}$ V/m) in this work, which is small enough to satisfy linear response criteria and large enough to avoid noticeable numerical error caused by small denominators.

The shape of the calculated spectra strongly depends on the number of atomic configurations used. Figure 2 displays the Raman spectra of the Pc structure at 210 GPa as an illustrative example. It shows that the calculated spectrum is a broad band when the number of atomic configurations used is small, which is similar to what was observed in Ref. [27]. After an average of 2000 configurations, the spectra start to display the feature of sharp peaks, and the peak feature can be well captured after an average of at least 3000 configurations.

B. Simulation details

First-principles Born-Oppenheimer molecular dynamics simulations are carried out on high-pressure solid-hydrogen phases III and IV with the QBOX [38] and QUANTUM ESPRESSO (QE) packages [39]. The Perdew-Burke-Ernzerhof (PBE) generalized gradient approximation (GGA) [40] exchange-correlation functional along with optimized norm-conserving Vanderbilt pseudopotentials [41] are used. A plane-wave cutoff of 70 Ry and a threshold for convergence of self-consistent electronic iterations of 1×10^{-6} hartrees are adopted. The atomic configurations contain 768 hydrogen atoms in order to mitigate the finite-size effects. Only the Γ point is used to sample the Brillouin zone. All the computational parameters are sufficient to converge the results with a total energy error smaller than 3.7 meV/atom and frequency errors of the spectra smaller than 20 cm^{-1}. Periodic boundary conditions and a time step of 5 a.u. (1 a.u. $= 0.048377$ fs) are applied to all simulations.

Quantum Monte Carlo combined with anharmonic vibrational calculations by Drummond *et al.* [42] showed that the structures with the lowest enthalpy for phases III and IV of hydrogen are the $C2/c$ and Pc structures, respectively. DFT calculations with the PBE functional [20] can also describe these structures as the most stable ones and are thus employed by us. Note that a hcp $P6_3/m$ structure, which was suggested by Azadi *et al.* [43] as an enthalpically competing structure of phase III below 220 GPa at zero temperature, is not considered in the current work because of the limited computational

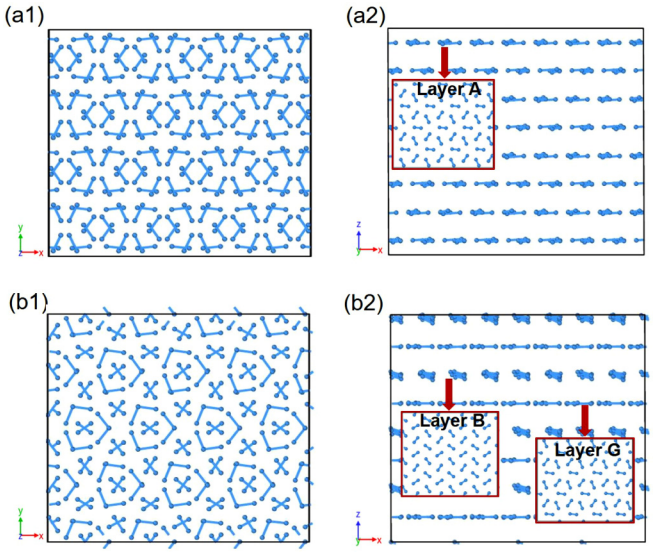

FIG. 1. (a1) Top and (a2) side views (eight layers in total) of the simulated 768-atom $C2/c$ cell. (b1) Top and (b2) side views (eight layers in total) of the simulated 768-atom Pc cell. The insets in (a2) and (b2) illustrate the top views of a single layer in $C2/c$ and Pc, respectively.

capacity of the FPMD method to deal with the PBE0 hybrid functional [44]. A supercell of the $4 \times 2 \times 2$ $C2/c$ primitive cell consisting of 768 atoms [Figs. 1(a1) and 1(a2)] is used as the initial configuration for phase III, the temperature is fixed at 100 K, and four independent simulations are conducted at 180, 220, 260, and 300 GPa. A supercell of the $4 \times 1 \times 2$ Pc primitive cell consisting of 768 atoms [Figs. 1(b1) and 1(b2)] is used as the initial configuration for phase IV. The primitive cell of the Pc structure is a four-layer monoclinic cell with the BGBG stacking pattern and contains 96 atoms. Layer B

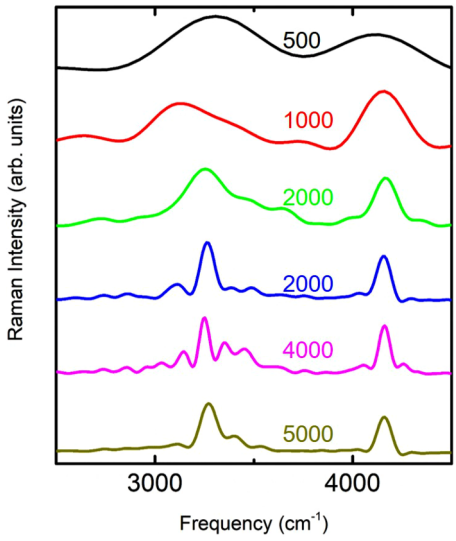

FIG. 2. Raman spectra of the Pc structure at 210 GPa calculated using different numbers of atomic configurations extracted from FPMD simulations. The configuration numbers are marked above the lines.

TABLE I. IR lattice phonon (IR1) and vibron (IR2) frequencies of the $C2/c$ structure at 300 GPa and different temperatures calculated using FPMD and DFPT methods.

Method	Temperature (K)	IR1 (cm^{-1})	IR2 (cm^{-1})
DFPT (Pickard *et al.* [20])	0	2120	4043
DFPT (this work)	0	2117	4036
FPMD (this work)	1	2100	4029
FPMD (this work)	100	2047	4082
FPMD (this work)	200	2021	4174

is a Br_2-like strongly bonded and freely rotating hydrogen molecule layer, while layer G is a weakly bonded layer that has a graphenelike structure. The temperature is fixed at 300 K, and four independent simulations are carried out at 210, 230, 250, and 270 GPa. Our simulations do not include the proton zero-point motion considering that nuclear quantum effects in phases III and IV are less important than those in phases I and II and including them will not qualitatively change the spectra of phases III and IV [30–33].

The finite-temperature IR and Raman spectra are extracted from FPMD simulations with QBOX, which can accurately and efficiently predict the response of complex and disordered systems to electric fields by first-principles methods and enables on-the-fly calculations of dipole moments and polarizabilities in FPMD [38]. Considering the lack of experimental lattice parameters, the cell lengths are determined from FPMD simulations in an isothermal-isobaric ensemble (NPT) in the QE package. The simulation procedures are as follows: (1) Variable-cell relaxations are conducted in the QE package in order to obtain the relaxed atomic positions and cell lengths at the fixed pressures and 0 K. (2) The structures are simulated in an NPT ensemble for 1.21 ps to achieve an equilibrium state. Therefore, we obtain the cell lengths (listed in Table II) at their corresponding temperatures and pressures. (3) The structures are then simulated in an NVT ensemble for 1.21 ps with QBOX and with the cell lengths obtained from the second step. The temperature is controlled by the Bussi-Donadio-Parrinello thermostat [45] and is adjusted every 100 steps. (4) The structures are subsequently equilibrated in an NVE ensemble for another 1.21 ps in QBOX. (5) The dipole moments and polarizabilities are extracted from the configurations of subsequent FPMD simulations every ten steps for the calculations of the IR and Raman spectra. About 5000 configurations are extracted in each simulation, corresponding to lengths of the trajectories of 12 ps.

To verify the finite-temperature effect included in the FPMD results is a genuine physical effect, we examine the temperature dependency of the spectra frequencies using the $C2/c$ structure at 300 GPa as an example. Table I displays IR lattice phonon (IR1) and vibron (IR2) frequencies calculated at increasing temperatures. The DFPT calculations are also presented as references at zero temperature. The calculation shows that the FPMD frequencies go back to the DFPT results at a low temperature close to zero, and the frequencies gradually depart from the DFPT results with the increase of temperature. This shows that the frequency shift at finite temperatures does not originate from numerical

TABLE II. X, Y, and Z cell lengths of the 768-atom $C2/c$ and Pc cells at different pressures obtained from the FPMD simulations in an NPT ensemble.

Structure	Pressure (GPa)	X (Å)	Y (Å)	Z (Å)
$C2/c$	180	12.13	10.57	10.85
$C2/c$	220	11.80	10.33	10.52
$C2/c$	260	11.53	10.11	10.26
$C2/c$	300	11.34	9.91	10.02
Pc	210	11.89	10.42	10.61
Pc	230	11.73	10.33	10.44
Pc	250	11.66	10.16	10.31
Pc	270	11.49	10.08	10.19

artifacts. Otherwise, the FPMD frequencies at a temperature close to zero will be significantly different from those calculated from the DFPT method.

III. RESULTS AND DISCUSSION

In the FPMD simulations, both $C2/c$ and Pc structures vibrate around their initial configurations, suggesting that these two structures are stable under the simulated conditions. Table II shows the cell lengths of the $C2/c$ and Pc structures, which decrease with increasing pressures in all three directions. Only one x-ray diffraction experiment of high-pressure hydrogen up to 183 GPa [17] is available to extract structural information. Therefore, we compare the $C2/c$ cell lengths at 180 GPa obtained from our FPMD simulation in the NPT ensemble with this experiment and find the errors are less than 2% in all directions.

Figure 3(a) shows the Raman spectra of the Pc phase extracted from the FPMD simulation in this work and those calculated using DFPT [20], together with the experimental Raman spectra [5] of phase-IV hydrogen at 250 GPa. The low-frequency vibron mode and the high-frequency vibron mode are denoted as $\nu 1$ and $\nu 2$, respectively. Importantly, our spectra reproduce the linewidths for both $\nu 1$ and $\nu 2$ modes in the experiment due to inclusion of the anharmonic temperature effects, while the two modes in the spectra obtained from the zero-temperature DFPT method do not exhibit a linewidth. The frequencies of the $\nu 2$ mode from this work (4143 cm^{-1}) and the DFPT method [20] (4170 cm^{-1}) are both in excellent agreement with the experiment [5] (4141 cm^{-1}). However, the frequencies of the $\nu 1$ mode from DFPT [20] (2770 cm^{-1}) is 510 cm^{-1} smaller than the experimental value [5] (3280 cm^{-1}), while the frequency of the $\nu 1$ mode from this work (3078 cm^{-1}) is only 202 cm^{-1} smaller than the experimental value [5]. The reduced error of frequency and the improved linewidth demonstrate that our method is more suitable to provide a direct comparison of the simulated spectra with the experimental spectra at finite temperatures. As to the mode intensity, it is difficult to directly compare the amplitude of peaks obtained in theory to the experimental value because the experimental intensity of the high-frequency mode was underestimated due to the lower sensitivity of the experimental detecting equipment at a higher frequency [46]. Figure 3(b) illustrates the Raman spectra of the Pc structure calculated in this work at 210, 230, 250, and 270 GPa. We find that the frequency and linewidth of the $\nu 2$ mode hardly change with the pressure, while the spectra of the $\nu 1$ mode soften and broaden dramatically with increasing pressures, which is in line with experimental findings [14,47,48]. All of the above evidence indicates that the temperature effect plays an important role in high-pressure hydrogen spectra and should be included in theoretical calculations.

The Raman spectra, pair correlation functions, and mean-square displacements (MSDs) of layers B and G of the Pc structure are further studied to understand their

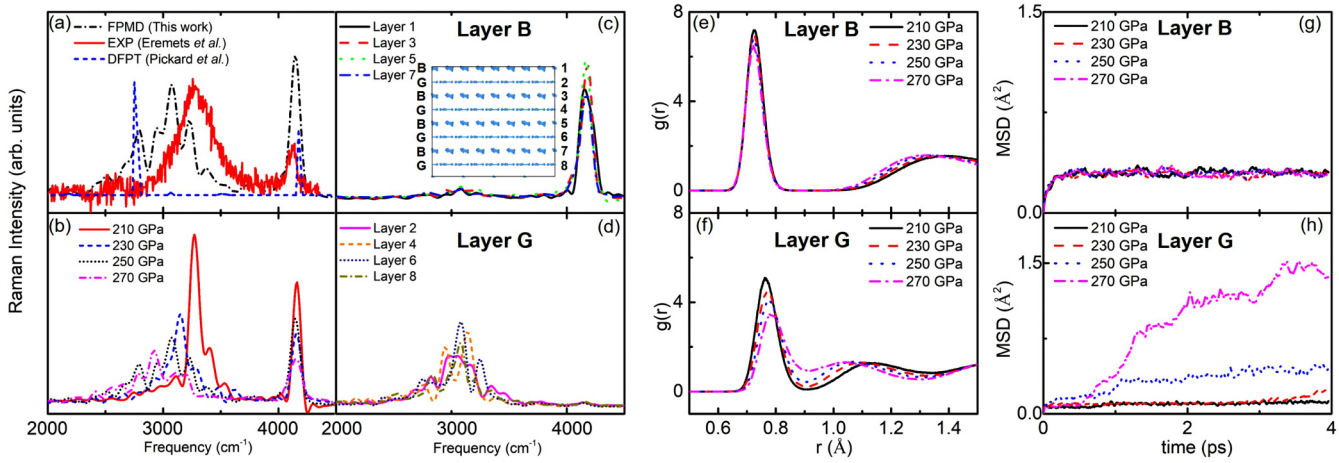

FIG. 3. (a) Raman spectra of solid hydrogen at 250 GPa. The black dash-dotted line is extracted from FPMD simulation of the Pc structure at 300 K in this work. The blue dashed line is calculated using the zero-temperature DFPT method with Pc structure by Pickard *et al.* [20]. The solid red line was obtained in experiment at 300 K by Eremets and Troyan [5]. (b) Raman spectra of the Pc structure calculated in this work at 210, 230, 250, and 270 GPa. The temperature is set to 300 K. (c) Raman spectra of layers 1, 3, 5, and 7 of the Pc structure calculated at 300 K and 250 GPa in this work. (d) Raman spectra of layers 2, 4, 6, and 8 of the Pc structure calculated at 300 K and 250 GPa in this work. The inset in (c) shows the sequence numbers for two types (B and G) of layers. Pair correlation functions of (e) layer B and (f) layer G of the Pc structure extracted from our FPMD simulations at 210, 230, 250, and 270 GPa. Mean-square displacements of (g) layer B and (h) layer G of the Pc structure obtained from our FPMD simulations at 210, 230, 250, and 270 GPa.

different structural and dynamic properties. Figures 3(c) and 3(d) display the decomposed Raman spectra of a single layer B and layer G, respectively. As illustrated in these figures, the two layers exhibit different vibrational behaviors; the $\nu 1$ and $\nu 2$ modes are mainly contributed by layers G and B, respectively. Moreover, we observe that the spectra of layer B slightly contribute to $\nu 1$ peaks, while the spectra of layer G also have small components of $\nu 2$ peaks, which indicates a weak coupling between layer B and layer G. Figure 3(e) illustrates the pair correlation functions of layer B, where the first peak is well separated from the second peak. The first peak is located at 0.72 Å and hardly changes at different pressures, suggesting that the hydrogen-hydrogen covalent bonds in layer B are well defined. The second peak represents the distance between hydrogen molecules. We find that the second peak shifts inwards at higher pressures, which is due to the fact that the cell lengths decrease with increasing pressure as obtained from FPMD simulations (Table II). Interestingly, the increased pressure does not change the covalent bond length of hydrogen molecules. This is in accordance with the fact that the frequency of the $\nu 2$ mode represents the short-range intramolecular vibration [46], which explains the invariance of the $\nu 2$ mode frequency in the experimental Raman spectra. However, Fig. 3(f) shows the pair correlation functions of layer G, and we find that there are no clear boundaries between the first and second peaks. Instead, layer G exhibits liquidlike behaviors, and the hydrogen-hydrogen pair distances vary smoothly from the first peak (0.763 Å at 210 GPa, 0.772 Å at 230 GPa, 0.778 Å at 250 GPa, and 0.785 Å at 270 GPa) to the second peak (1.126 Å at 210 GPa, 1.106 Å at 230 GPa, 1.069 Å at 250 GPa, and 1.058 Å at 270 GPa). Furthermore, the positions of the first peaks indicate that the bond length increases with the pressure, suggesting that the covalent bonds in layer G are weakened with increasing pressure. As is known, weaker covalent bonds vibrate with lower frequencies, which explains the decrease of the $\nu 1$ mode frequency with increasing pressure. The MSD characterizes the diffusive behavior of the system and can be calculated as $\mathrm{MSD} = \frac{1}{N}\sum_{i=0}^{N}\langle[r_i(t) - r_i(0)]^2\rangle$, where N is the number of atoms in layer B or layer G, $r_i(t)$ is the position of the ith atom at time t, and $\langle\cdots\rangle$ represents the ensemble average. Figure 3(g) shows that the MSD of layer B reaches a constant in a short time, which indicates that there is no diffusion behavior of hydrogen atoms in layer B as observed in our trajectories. On the contrary, the MSD of layer G, as illustrated in Fig. 3(h), keeps increasing with simulation time. More importantly, the diffusion behavior in layer G increases with pressure, which explains the broadening of the $\nu 1$ mode with pressure.

The pressure dependence of IR and Raman frequencies of phases III and IV is displayed in Fig. 4, where the two most intense IR-active modes (a lattice phonon mode IR1 and a vibron mode IR2) and one Raman vibron mode (RAMAN) of phase III are presented. For IR1, the frequencies calculated using our method and the DFPT method [19] both agree well with experiment [12]. For RAMAN and IR2, the frequencies calculated using the DFPT method [19] are about 200 cm^{-1} smaller than experiment [6,12], while the frequencies calculated by our method are in excellent agreement with experiment [6,12], which supports the theory that $C2/c$ is the crystalline structure of phase III. Figure 4(b) shows the $\nu 1$ and $\nu 2$ Raman vibron modes of phase IV, which are indicated as RAMAN1 and RAMAN2, respectively. The frequencies of the $\nu 2$ mode calculated by our method and the DFPT method [20] are both in excellent agreement with experiment [47]. However, the frequencies of the $\nu 1$ mode calculated by the DFPT method [20] are about 500 cm^{-1} smaller than the experimental values [47], while our results are only about 200 cm^{-1} smaller than the experimental values [47]. We consider that the calculated spectra of both $C2/c$ and layer B of Pc are in excellent agreement with experiment because in these structures the covalent bonds are well captured by the PBE functional. However, the covalent bonds, which are between hydrogen atoms inside hydrogen molecules, in layer G of Pc are weaker than those in layer B because the hydrogen atoms in layer G are more disordered and liquidlike, which suggests that the van der Waals interactions may be important in describing atomic interactions in layer G. However, the PBE-GGA functional, which is used in both our simulation and the AIRSS by Pickard *et al.* [20], cannot describe the intermediate- and long-range van der Waals interactions. This may lead to the discrepancy between the PBE-GGA-predicted Pc structure and the real crystalline structure of hydrogen phase IV. The smaller frequencies of the $\nu 1$ mode of the Pc structure compared with those of experiments suggests that the bond lengths in layer G of the Pc structure are longer than the experimental values. Therefore, we suspect that the PBE-GGA-predicted Pc structure is different from the real crystalline structure of hydrogen phase IV to some extent. Moreover, Fig. 4 shows the frequencies of the vibron modes (RAMAN, IR2, RAMAN1, and RAMAN2) decrease with increasing pressures, while the frequencies of the lattice phonon mode (IR1) increase with increasing pressures. This is due to the fact that the increasing pressure decreases the distances between hydrogen molecules, which makes the intramolecular stretches become easier and the lattice vibrations become harder.

The diffusion processes in layer G of phase IV, which contribute to the large linewidth of the $\nu 1$ mode [28,46,49–51], are found to be confined in plane and are displayed in Fig. 5. Liu *et al.* [28] briefly discussed two diffusion processes in layer G. In this work, three diffusion processes are identified and discussed in detail. Figures 5(a) and 5(b) show the first category of diffusion process, rotation of hydrogen ring clusters: Any three molecules around a circle [blues circles in Fig. 5(a) and purple circles in Fig. 5(b)] form a ring cluster and rotate along the circle. In both processes $1'$ and $1''$, some of the ring clusters rotate clockwise (indicated by the black arrows on the circles), while some of the clusters rotate anticlockwise (indicated by the red arrows on the circles), and the rest of the ring clusters do not rotate. During this rotation process, the two adjacent atoms [the red and green atoms in Fig. 5(a) and the purple and orange atoms in Fig. 5(b)] remain adjacent and stay in the same ring cluster. Figures 5(a)–5(c) illustrate the second type of diffusion process, reconstruction of hydrogen ring clusters: This is a process that converts the ring clusters formed in process $1'$ to those ring clusters found in process $1''$. Before a time of 5.58 ps, three molecules around a blue circle form a cluster and rotate, but the clusters experience recombination after a time of 5.58 ps: The three

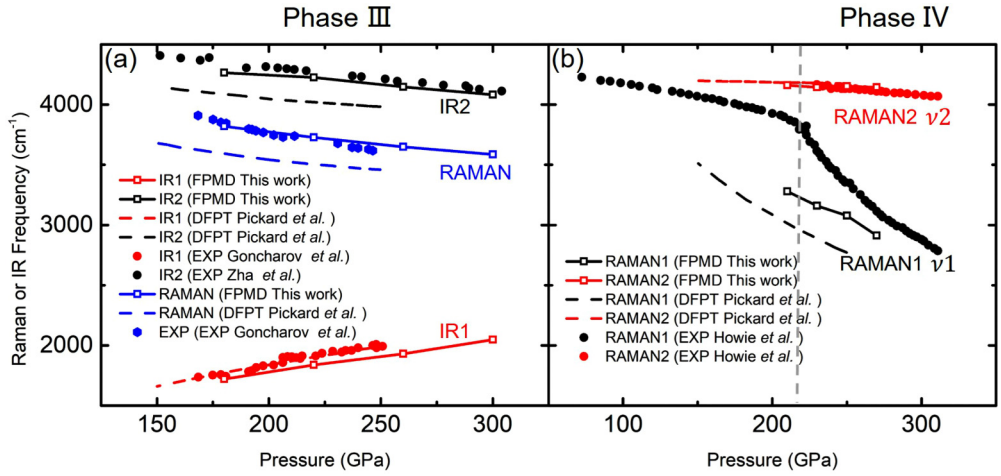

FIG. 4. Pressure dependence of IR and Raman frequency of (a) phase III and (b) phase IV solid hydrogen. The solid lines with open symbols represent our FPMD results, the dashed lines represent the DFPT results from Refs. [19,20], and the solid symbols represent the experimental results from Refs. [6,12,47].

molecules around the blue circles stop rotating, and the three molecules around the purple circle form new clusters and start to rotate. Although in both processes 1′ and 1″ two adjacent atoms remain adjacent and stay in the same cluster, combining these two processes, the two atoms [the red and yellow atoms in Fig. 5(c)] originally adjacent are separated into different ring clusters. We suspect this process is the underlying mechanism that governs the different patterns in the collected trajectories of layer G observed by Liu *et al.* [28], which they conclude are the reconstruction of all molecules every 2–3 ps. Figure 5(d) displays the third type of process, self-organization of hydrogen ring clusters: One hydrogen molecule (the red and green atoms) flips perpendicular to the plane direction and stays in the same ring cluster by simply exchanging the positions of two covalently bonded atoms. As a result, the two adjacent atoms that are not bonded by covalent bonds (the red and orange atoms) in one cluster remain in the same cluster, but they are no longer adjacent. Through the three types of diffusion processes, one atom can travel freely in the same layer, and the covalent bonds are very short-lived. As shown in Fig. 5, even though any two atoms within a distance as large as 0.9 Å are connected by a covalent bond, some hydrogen atoms are still isolated. This phenomenon is in accordance with the pair correlation function [Fig. 4(f)] and indicates the hydrogen molecules in layer G have weaker covalent bonds than those in layer B

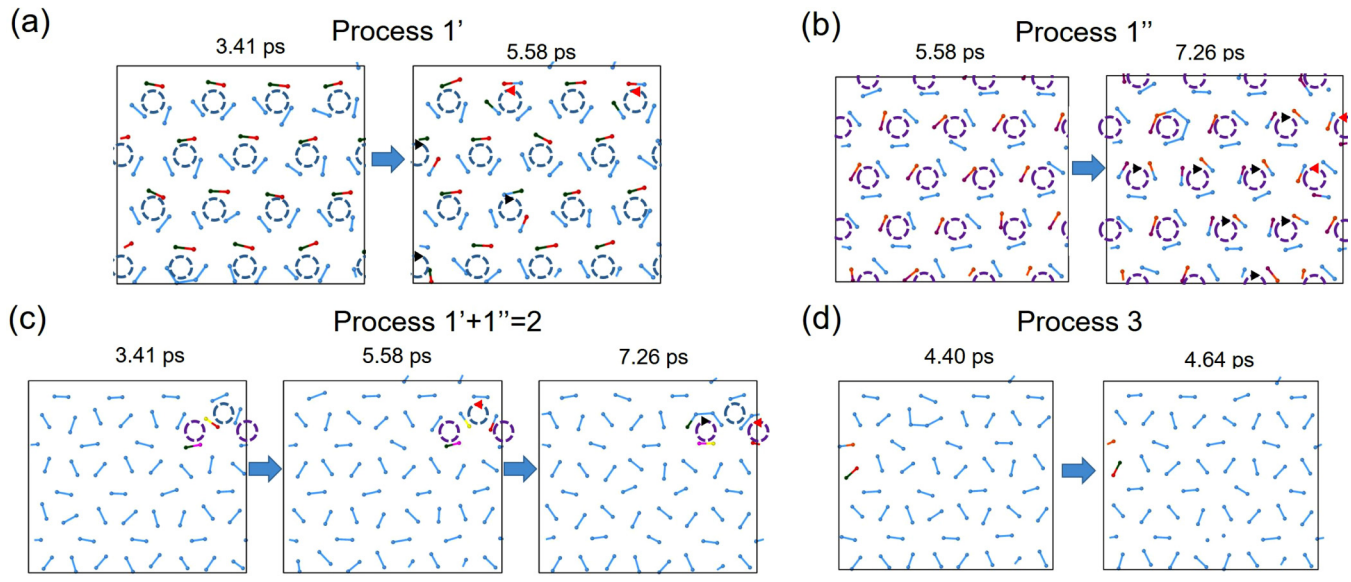

FIG. 5. Snapshots of a single layer, G, of the *Pc* structure extracted from the FPMD simulation in an *NVE* ensemble at 270 GPa. A selected number of atoms are marked with different colors in order to trace them, and any two atoms within 0.9 Å are considered to be connected by a covalent bond. The characteristic length of 0.9 Å is the position of the first valley in the pair correlation functions of layer G [Fig. 3(f)]. Hence, the covalently bonded hydrogen molecules are well separated from the rest of the atoms, which is beneficial to the visualization of the diffusion processes.

and start to dissociate into hydrogen atoms with increasing pressure. Hence, we suspect that phase IV may be a transition phase between the molecular phase and atomic phase of hydrogen.

IV. CONCLUSION

In conclusion, we calculated the finite-temperature IR and Raman spectra of the theoretically proposed candidate structures $C2/c$ and Pc for solid hydrogen by Fourier transforms of the TCFs of dipole moments and polarizabilities, respectively. The dipole moments and polarizabilities are extracted from FPMD trajectories of 768-atom supercells. The $C2/c$ structure is simulated at 100 K and pressures of 180, 220, 260, and 300 GPa. The Pc structure is simulated at 300 K and pressures of 210, 230, 250, and 270 GPa. The linewidth and some frequencies (the IR vibron and Raman vibron frequencies for phase III and the $\nu 1$ Raman vibron frequencies for phase IV) calculated in this work are in better agreement with experiment than the spectra obtained from the DFPT method at zero temperature, indicating the necessity of including the temperature effect in theoretical calculations of high-pressure solid-hydrogen spectra.

The agreement of the calculated spectra of the $C2/c$ structure with the experimental result supports the theory that the $C2/c$ structure is the crystalline structure of phase III. The disagreement between the spectra of the Pc structure and experimental spectra shows that the predicted Pc structure, which is the stable structure of phase IV in our FPMD simulations with the PBE exchange-correlation functional, differs from the real crystalline structure of phase IV in atomic structures to some extent.

Examining the Raman spectra, pair correlation functions, and mean-square displacements of different layers in the Pc structure confirmed that the high-frequency vibron mode is contributed by layer B and the low-frequency vibron mode is contributed by layer G, where layer B is a strongly bonded layer and layer G is a weakly bonded diffusive layer. Moreover, the three diffusion processes in layer G of the Pc structure observed in our simulation suggest the short lifetime of the hydrogen-hydrogen covalent bonds.

ACKNOWLEDGMENTS

This work is supported by the Science Challenge Project No. TZ2016001, the NSFC (Grants No. 21503019 and No. 11625415), the NSAF (Grants No. U1530258 and No. U1530113). Part of the calculations are supported by the Special Program for Applied Research on Super Computation of the NSFC-Guangdong Joint Fund (the second phase) under Grant No. U1501501.

[1] H.-k. Mao and R. J. Hemley, Rev. Mod. Phys. **66**, 671 (1994).
[2] J. M. McMahon, M. A. Morales, C. Pierleoni, and D. M. Ceperley, Rev. Mod. Phys. **84**, 1607 (2012).
[3] A. F. Goncharov, R. T. Howie, and E. Gregoryanz, Low Temp. Phys. **39**, 402 (2013).
[4] P. Loubeyre, F. Occelli, and R. LeToullec, Nature (London) **416**, 613 (2002).
[5] M. Eremets and I. Troyan, Nat. Mater. **10**, 927 (2011).
[6] C.-S. Zha, Z. Liu, and R. J. Hemley, Phys. Rev. Lett. **108**, 146402 (2012).
[7] R. P. Dias and I. F. Silvera, Science **355**, 715 (2017).
[8] P. Dalladay-Simpson, R. T. Howie, and E. Gregoryanz, Nature (London) **529**, 63 (2016).
[9] E. Wigner and H. Á. Huntington, J. Chem. Phys. **3**, 764 (1935).
[10] N. W. Ashcroft, Phys. Rev. Lett. **21**, 1748 (1968).
[11] R. J. Hemley and H. K. Mao, Phys. Rev. Lett. **61**, 857 (1988).
[12] A. F. Goncharov, E. Gregoryanz, R. J. Hemley, and H.-k. Mao, Proc. Natl. Acad. Sci. U.S.A. **98**, 14234 (2001).
[13] M. I. Eremets, I. A. Troyan, and A. P. Drozdov, arXiv:1601.04479.
[14] C.-s. Zha, R. E. Cohen, H.-k. Mao, and R. J. Hemley, Proc. Natl. Acad. Sci. U.S.A. **111**, 4792 (2014).
[15] R. P. Dias, O. Noked, and I. F. Silvera, arXiv:1605.05703.
[16] P. Loubeyre, R. LeToullec, D. Hausermann, M. Hanfland, R. Hemley, H. Mao, and L. Finger, Nature (London) **383**, 702 (1996).
[17] Y. Akahama, M. Nishimura, H. Kawamura, N. Hirao, Y. Ohishi, and K. Takemura, Phys. Rev. B **82**, 060101(R) (2010).
[18] P. Hohenberg and W. Kohn, Phys. Rev. **136**, B864 (1964).
[19] C. J. Pickard and R. J. Needs, Nat. Phys. **3**, 473 (2007).
[20] C. J. Pickard, M. Martinez-Canales, and R. J. Needs, Phys. Rev. B **85**, 214114 (2012).
[21] B. Monserrat, R. J. Needs, E. Gregoryanz, and C. J. Pickard, Phys. Rev. B **94**, 134101 (2016).
[22] K. A. Johnson and N. Ashcroft, Nature (London) **403**, 632 (2000).
[23] C. J. Pickard and R. Needs, Phys. Status Solidi B **246**, 536 (2009).
[24] C. J. Pickard and R. Needs, J. Phys.: Condens. Matter **23**, 053201 (2011).
[25] S. Baroni, S. De Gironcoli, A. Dal Corso, and P. Giannozzi, Rev. Mod. Phys. **73**, 515 (2001).
[26] I. B. Magdău and G. J. Ackland, Phys. Rev. B **87**, 174110 (2013).
[27] R. Singh, S. Azadi, and T. D. Kühne, Phys. Rev. B **90**, 014110 (2014).
[28] H. Liu, J. Tse, and Y. Ma, J. Phys. Chem. C **118**, 11902 (2014).
[29] C. Zhang, D. Donadio, and G. Galli, J. Phys. Chem. Lett. **1**, 1398 (2010).
[30] H. E. Lorenzana, I. F. Silvera, and K. A. Goettel, Phys. Rev. Lett. **64**, 1939 (1990).
[31] I. I. Mazin, R. J. Hemley, A. F. Goncharov, M. Hanfland, and H.-k. Mao, Phys. Rev. Lett. **78**, 1066 (1997).
[32] X.-Z. Li, B. Walker, M. I. Probert, C. J. Pickard, R. J. Needs, and A. Michaelides, J. Phys.: Condens. Matter **25**, 085402 (2013).
[33] M. A. Morales, J. M. McMahon, C. Pierleoni, and D. M. Ceperley, Phys. Rev. Lett. **110**, 065702 (2013).

[34] D. McQuarrie, *Statistical Mechanics* (University Science Books, Sausalito, CA, 2000).
[35] N. Marzari and D. Vanderbilt, Phys. Rev. B **56**, 12847 (1997).
[36] M. Stengel and N. A. Spaldin, Phys. Rev. B **73**, 075121 (2006).
[37] Q. Wan, L. Spanu, G. A. Galli, and F. Gygi, J. Chem. Theory Comput. **9**, 4124 (2013).
[38] F. Gygi, IBM J. Res. Dev. **52**, 137 (2008).
[39] P. Giannozzi, S. Baroni, N. Bonini, M. Calandra, R. Car, C. Cavazzoni, D. Ceresoli, G. L. Chiarotti, M. Cococcioni, I. Dabo *et al.*, J. Phys.: Condens. Matter **21**, 395502 (2009).
[40] J. P. Perdew, K. Burke, and M. Ernzerhof, Phys. Rev. Lett. **77**, 3865 (1996).
[41] M. Schlipf and F. Gygi, Comput. Phys. Commun. **196**, 36 (2015).
[42] N. D. Drummond, B. Monserrat, J. H. Lloyd-Williams, P. L. Ríos, C. J. Pickard, and R. J. Needs, Nat. Commun. **6**, 7794 (2015).
[43] S. Azadi, W. Foulkes, and T. D. Kühne, New J. Phys. **15**, 113005 (2013).
[44] S. Azadi and T. D. Kühne, JETP Lett. **95**, 449 (2012).
[45] G. Bussi, D. Donadio, and M. Parrinello, J. Chem. Phys. **126**, 014101 (2007).
[46] R. T. Howie, T. Scheler, C. L. Guillaume, and E. Gregoryanz, Phys. Rev. B **86**, 214104 (2012).
[47] R. T. Howie, C. L. Guillaume, T. Scheler, A. F. Goncharov, and E. Gregoryanz, Phys. Rev. Lett. **108**, 125501 (2012).
[48] P. Loubeyre, F. Occelli, and P. Dumas, Phys. Rev. B **87**, 134101 (2013).
[49] A. F. Goncharov, J. S. Tse, H. Wang, J. Yang, V. V. Struzhkin, R. T. Howie, and E. Gregoryanz, Phys. Rev. B **87**, 024101 (2013).
[50] H. Liu and Y. Ma, Phys. Rev. Lett. **110**, 025903 (2013).
[51] H. Liu, L. Zhu, W. Cui, and Y. Ma, J. Chem. Phys. **137**, 074501 (2012).